Coarse Grained Simulations of Local Anesthetics Encapsulated into a Liposome

Mónica Pickholz*,† and Giovanni Giupponi*,‡

Consejo Nacional de Investigaciones Científicas y Técnicas (CONICET) and Facultad de Farmacia y Bioquímica, Universidad de Buenos Aires, Junin 954 RA-1053, Argentina, and Department de Física Fonamental, Universitat de Barcelona, Carrer Marti i Franques, 08028 Barcelona, Spain

Received: September 23, 2009; Revised Manuscript Received: February 12, 2010

We investigated the encapsulation of prilocaine (PLC), an aminoamide local anesthetic widely used in dentistry, into a small unilamellar liposome. We extended a recently developed coarse grained model to access the problem relevant time and length scales. Molecular dynamics (MD) simulations for different protonation states of the PLC captured important features of the PLC−vesicle interactions. We found that all neutral PLC molecules (nPLC) rapidly diffuse into the hydrophobic region of the vesicle adopting an asymmetric bimodal density distribution, with nPLC molecules jumping between the internal and external vesicle monolayers. Protonated PLC molecules (pPLC) initially placed in water were instead only found on the external monolayer, with a high rate of exchange with the water phase and no access to the inner part of the liposome. Although electrostatic interaction between pPLC tails and oppositely charged lipid head groups is shown to be structured, hydrophobicity is the driving force of PLC drug absorption within the liposome. Our simulations also show that a major percentage of pPLC remains trapped within the interior water phase of the liposome when starting from a configuration with pPLC distributed within the lipid membrane. This suggests that at low pH liposome−PLC complexes and therefore drug efficacy can strongly depend on the preparation procedure.

1. Introduction

Relief of localized pain is a challenging problem in medical and odontological research. Local anesthetic (LA) agents used to relieve pain symptoms are characterized by limited duration of analgesia and may result in both systemic and local toxicity.[1] However, many of the pharmacological properties of conventional drugs can be improved through the use of drug delivery systems, which include particulate carriers, composed primarily of lipids or polymers, and their associated therapeutics.[2,3] For instance, LAs encapsulated in liposomes have been shown to gradually release the drug, obtaining a prolonged duration of the anesthetic action and reducing the central nervous or cardiovascular system toxicity.[4]

Liposomes are small lipid vesicles of spherical shape that contain a core of aqueous solution. They can spontaneously form from lipid dispersed in water[3] and are used as a versatile tool in biology, biochemistry, and medicine. Their composition can vary from naturally derived phospholipids with mixed lipid chains like egg phosphatidylethanolamine to pure lipid components like 1-palmitoyl-2-oleoyl-*sn*-glycero-3-phosphatidylcholine (POPC). The mean diameter of the smallest unilamellar liposomes is on the order of 25−30 nm. Liposomes are employed as microcarriers for a big variety of compounds such as drug molecules, proteins, nucleotides, and plasmids.[3] As LAs have a high affinity for the cellular membrane because of their amphiphatic nature, they are a convenient system to encapsulate and transport LAs.

A better understanding of the mechanisms of drug encapsulation can help to improve the design of more effective drug delivery protocols. Molecular dynamics (MD) is a useful tool to investigate the interactions of different drugs with membranes,[5,6] providing fine grained molecular detail that is often not accessible to experiments.[7] Recently, drug controlled processes have been studied by means of MD simulations;[8,9] however, systematic studies using fully atomistic MD are computationally very expensive, and therefore often cannot access relevant length and time scales.[10]

The use of simplified, coarse grained (CG) models, where degrees of freedom are removed mapping a few atoms into a unique site, helps to relieve the burden of fully atomistic simulations while still retaining sufficient physical detail to accurately simulate cooperative and mesoscopic-scale phenomena of experimental and theoretical interest. In this work, we employ version 2.0 of the MARTINI coarse grained force field[11] (hereafter referred to as MARTINI), which has been successfully used to investigate a variety of drug-delivery-related phenomena such as self-assembly and fusion of liposomes,[12,13] translocation of fullerene particles through lipid membranes,[14] insertion of a protein into a lipid bilayer,[15,16] and diffusion of small molecules into lipid membranes.[17−19]

In the following sections, we investigate the encapsulation of prilocaine (PLC), a local anesthetic widely used in dentistry, into a small liposome through coarse grained MD simulations extending the MARTINI force field to include parameters for prilocaine. Despite its versatility, this CG force field has not been designed to provide a coarse graining model "out of the box" for all chemical moieties. However, in this work, we demonstrate that it is possible to extend its features and include other molecules such as PLC. In addition, to the best of our knowledge, LA absorption on a liposome has not been tackled with methods allowing one to follow the process at the microsecond scale, and we report here that extended MARTINI is well suited to investigate PLC absorption mechanisms and features.

The rest of the paper is organized as follows: In the following section, we provide simulation details. In section 3.1, we extend the CG force field to include PLC parameters comparing CG

† Universidad de Buenos Aires.
‡ Universitat de Barcelona.

10.1021/jp909148n
Published on Web 04/29/2010

with fully atomistic results for a flat POPC bilayer. As most LA molecules can be found in neutral and protonated form at physiological pH, we parametrize both cases in order to investigate the observed stronger affinity to lipid membranes of neutral species.[20] Results for PLC distributions are shown in section 3.2. Finally, in the last section, we draw our conclusions.

2. Simulation Details

In this work, we adopt a recently developed coarse graining model, referred to as the MARTINI force field,[11] to obtain a coarse grained description of our molecular systems. This method aims at a systematic and portable representation for water, phospholipids, and other small molecules in terms of a few building blocks, or CG particles, that interact with potential parameters optimized for use in a broad range of biomolecular applications. A four heavy atoms to one CG particle mapping rule is generally followed, and hydrogen atoms are neglected because of their small size and mass. This model considers four main types of CG particles: polar (P), nonpolar (N), apolar (C), and charged (Q).

The "native" CG topologies built and tested using the MARTINI force field[11] do not feature an explicit recipe for prilocaine molecules. However, the building chemical blocks of the force field permit the coarse grained representation of generic molecules to quite easily be extended, once the chemical characteristics such as polarity and charge distribution of constitutive moieties are known (see below). This CG force field has been shown to correctly describe a variety of macromolecular systems such as lipid bilayers,[11,21] phospholipid vesicles,[12,22] and membrane proteins.[15,16,23] For a detailed description of force features and parameters, see ref 11. In this work, the parameters for neutral and protonated PLC were chosen by chemical analogy among the particles already present in MARTINI, and then, the best matching type was chosen comparing results from CG and atomistic simulations.[24,25] The rest of the CG particles for lipids, water, and ions follow the standard force field.

We simulate the absorption of prilocaine molecules onto a POPC lipid vesicle. A preassembled POPE lipid vesicle[26] was used as a template to create a POPC vesicle changing the first coarse grained atom of POPE NH3 (type Qd) into NC3 (type Q0). The system was then solvated into a mixture of water particles and PLC molecules. The 224[33] cubic simulation box consists of a vesicle of 877 POPC lipids (254 and 623 for the internal and external monolayer, respectively), 81550 water particles, and 88 PLC (neutral or protonated) molecules. We generated three different starting configurations, depending on how we added PLC molecules to the mixture, as we explain below. Counterions were always added randomly in the water phase when required to ensure electroneutrality. For each starting configuration, we run 250 ns of equilibration in the NPT ensemble, followed by 1 μs in the NVT ensemble.

Risselada et al.[27] pointed out that fully equilibrated vesicle structures would require much longer (and at present unachievable) simulations to allow lipid flip-flopping. Nevertheless, they were able to allow lipid flip-flopping using membrane pores and obtained fully relaxed vesicle structures. For such structures, the ratio of inner versus outer leaflet lipid density can vary up to 4% when compared with vesicle structures obtained by other means. They also report that most metastable structures are "within the tails of the expected distribution". As we focus mainly on the drug behavior, our results are not affected by such differences.

The simulations were carried out with the GROMACS 4.0 simulation package,[28] using a simulation time step of 40 fs with a nonbonded and electrostatic cutoff of 12 Å. The reference temperature was set to 325 K using a Berendsen thermostat with a time constant of 1.0 ps. For NPT runs, Berendsen pressure coupling was used with a reference pressure of 1 bar, a time constant of 5.0 ps, and a compressibility of 3×10^{-5} bar^{-1}. On a computational note, we report that a fully atomistic representation of the same systems would need around a million atoms to be run with a typical simulation time step of 2 fs. As drug diffusion and adsorption phenomena involve characteristic scales of tens of nanometers and hundreds of nanoseconds, we conclude that extensive fully atomistic simulations reaching the microsecond of such phenomena are not practically possible even using the biggest supercomputers, leaving coarse grained force fields the only feasible models.

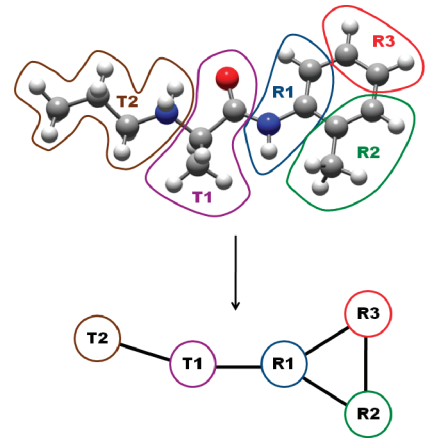

Figure 1. Sketch of atomistic to coarse grained mapping of prilocaine.

3. Results

3.1. PLC Force Field Parametrization. We have built a CG PLC molecule that preserves a number of key physical and structural features found using atomistic simulations.[25] We have not attempted to change any of the bead parameters of the MARTINI force field; rather, we have chosen at first the PLC CG sites by analogy with similar groups from Table 3 of ref 11, and then improved the agreement with atomistic simulation results following a trial and error procedure changing bead types.

The resulting mapping of PLC to CG particles represents the 36 (37) atoms of nPLC (pPLC) with five MARTINI particles, as shown in Figure 1. The bonded and nonbonded parameters for the R1, R2, and R3 head sites of the PLC neutral and protonated species were taken from the benzene parameters SC4 of ref 11. The mass of these sites, unlike ref 11, was set to be proportional to the number of non-hydrogen atoms, that is, 54 amu for R1 and R2 and 36 amu for R3. The parameters for the tail sites (T1 and T2) depend on the ionization state of the PLC molecule. For neutral PLC, we assigned the type Na (2-propane, nitromethane, proprionitrile, methylformate, propanal) and C2 (propane) for T1 and T2, respectively. For the protonated case, we assigned the type Q0 for both T1 and T2 sites, with charges of 0.4 and 0.6, respectively. Chloride counterions, when present, are represented by Qa site types.

We carried out several simulations of a POPC lipid bilayer containing PLC and compare the results with fully atomistic simulations from ref 25. The simulated lipid bilayer contained 120 fully hydrated POPC lipids (60 in each monolayer), 1400 water molecules, and 40 neutral or protonated PLC molecules. Chloride counterions were included to ensure electroneutrality for the case of pPLC. The parameters that lead to the best

TABLE 1: Parameters for CG Neutral and Protonated PLC[a]

atom number	type/MARTINI type	charge	building block
1	R_1/SC4	0.00	HC═CNH
2	R_2/SC4	0.00	H_3CC═CH
3	R_3/SC4	0.00	HC═CH
4	T_1/Na (Q0)	0.00 (0.40)	O═CCHCH$_3$
5	T_2/C2 (Q0)	0.00 (0.60)	NH(NH$_2$)CH$_2$CH$_2$CH$_3$

bonds *i*,*j*	length (nm)	K_{bond} (kJ mol^{-1} nm^{-2})
1,2	0.240	2000
1,3	0.240	2000
1,4	0.470	1250
2,3	0.240	2000
4,5	0.470	1250

angles *i*,*j*,*k*	angle (deg)	K_{angle} (kJ mol^{-1} rad^{-2})
1,4,5	120.0	25.0
1,3,2	60.0	100.0
1,2,3	60.0	100.0
2,1,4	140	25.0
2,1,3	60.0	100.0
3,1,4	140.0	25.0

[a] Values in parentheses correspond to protonated PLC when different from the neutral ones. MARTINI types, from ref 11, as well as the chemical structure corresponding to each site are also included.

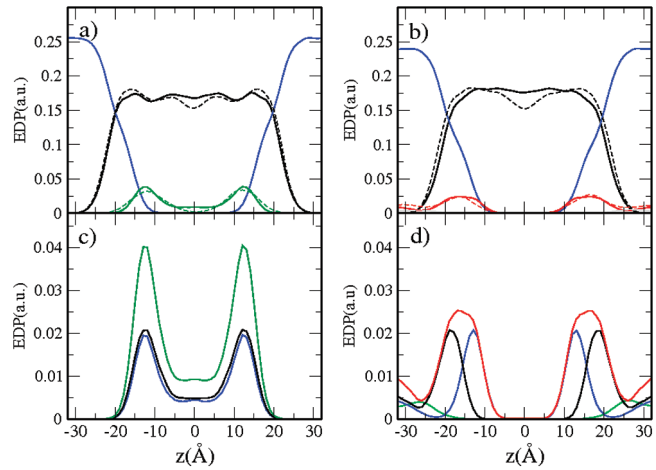

Figure 2. The electron density profile (EDP) of the different components of the bilayer as a function of the z coordinate, in (a) a bilayer containing neutral PLC and (b) a bilayer containing protonated PLC. The colors in parts a and b are blue for water, light green for POPC, dark green for nPLC, and red for pPLC. POPC and PLC EDPs from the atomistic simulations in parts a and b are shown as dashed lines. Panels c and d zoom into the EDP of PLCs and their components, head (brown) and tails (black) for protonated (red) and neutral (green), respectively. In part d), the chloride counterion distribution was also included in light green.

agreement between atomistic and CG simulations and therefore used for PLC absorption on a POPC vesicle are summarized in Table 1.

Experimentally, the interfacial ordering of the system can be measured through the electron density profile (EDP) normal to the bilayer with techniques such as X-ray or neutron scattering experiments.[29] We computed the EDP by time averaging the net charge $Q(z)$ (the nuclear charge corresponding to all of the atoms represented by each CG site) contained in the volume $\delta V(z)$ by

$$\mathrm{EDP}(z) \propto \left\langle \frac{Q(z)}{\delta V(z)} \right\rangle_t \quad (1)$$

Here, z is the (discrete) coordinate normal to the bilayer and the slice thickness is 0.1 Å. We have placed a Gaussian distribution of electrons on each site center with a variance equal to 2.0 Å. In Figure 2a and b, we show the EDPs of the different components of the nPLC and pPLC systems, respectively. In the same figures, we have included the POPC and PLC EDPs calculated from atomistic simulations[25] (dashed lines). We show in Figure 2a that nPLC is completely embedded into the POPC bilayer with little access to the lipid/water interface, with the nPLC EDP following a bimodal distribution, with two maxima at ∼12 Å from the central plane parallel to the membrane. We stress that the same values for the maxima are recovered from atomistic simulations and that differences between CG and atomistic EDPs are negligible.

For the pPLC case, shown in Figure 2b, our results correctly recover the distributions within the POPC bilayer of atomistic simulations, as pPLCs (in red) distribute between the water/lipid interface and the water phase, with no access to the bilayer center. The peaks of the pPLC distribution at the lipid/water interface are found at ∼17 Å from the bilayer center, in agreement with atomistic simulation results.[25] In Figure 2c and d, we plot the nPLC and pPLC EDP distributions, together with the EDPs of their tails (T1 and T2 groups) and heads (R1, R2, and R3 groups) only. For the nPLC case, the positions of maxima are the same for heads, tails, and the whole molecule; i.e., nPLCs do not have a specific orientation inside the membrane. On the contrary, for the pPLC case, the tail and head maxima are shifted by ∼5 Å, in good agreement with atomistic simulations that show a shift of ∼4 Å.[25] Tails are oriented facing the more polar region, because of the charged groups in the water/lipid region, and they do not show preferential orientation at the water phase, in agreement with the atomistic simulations.[25] In Figure 2d, we also show the EDP distribution of the chloride counterions included to compensate the charge of protonated PLCs. Chloride atoms are found in the bulk water and water/lipid head interface, with no access to the hydrophobic core. These findings are also confirmed by atomistic simulations.

Another feature observed in atomistic simulations is the ability of nPLC to cross from one monolayer to the other many times during a 20 ns simulation run. Our results using the CG PLC model can confirm this behavior, as the nonzero value of the nPLC EDP at the membrane center in Figure 2c suggests nPLC is not localized within the bilayer. On the other hand, Figure 2d does not show pPLC molecules in between monolayers, again in agreement with atomistic simulations.

We have demonstrated here that the chosen PLC parameters, listed in Table 1, are well-suited to reproduce semiquantitatively the main results of atomistic simulations and consequently experimental results, as atomistic MD simulations were essential for the interpretation of the observed saturation transfer difference (STD) experiments.[25] We conclude that our CG model is able to capture qualitative behavior of PLC molecules in lipids, and therefore can be used to effectively study systems that are computationally too expensive to be modeled with full atomistic detail, like drug encapsulation processes.

3.2. Absorption of PLC Molecules on a POPC Vesicle. We use the CG model to investigate the absorption of PLC molecules in a small (∼150 Å diameter) POPC vesicle. We generated three different starting configurations, depending on

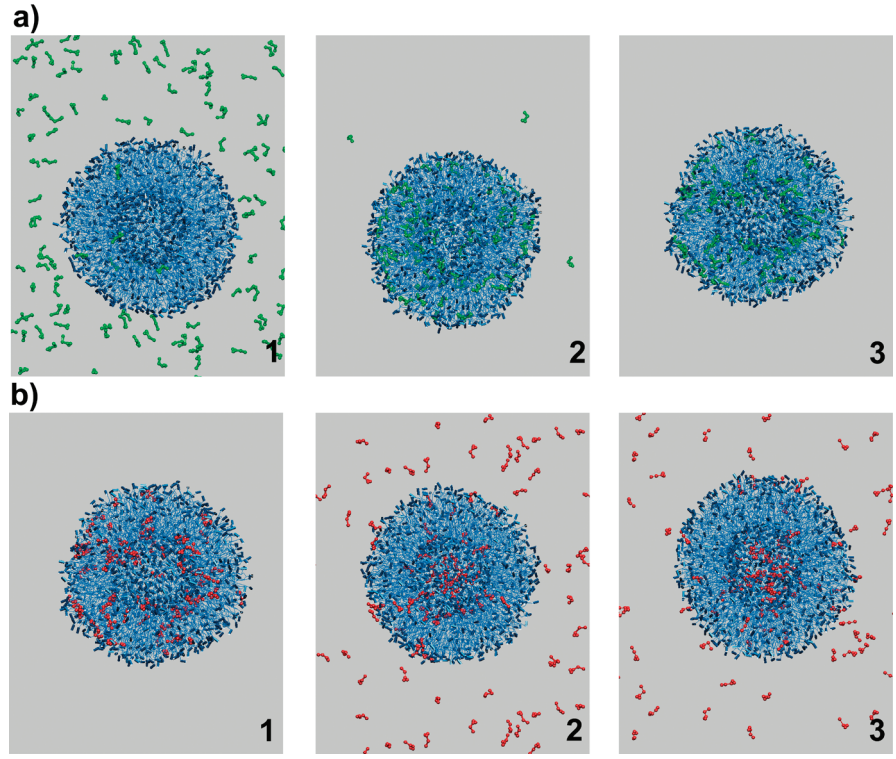

Figure 3. Snapshots from the molecular dynamics simulations of PLC in POPC vesicles: (a) nPLC-O; (b) pPLC-I. The snapshots correspond to the initial configuration (1, $t = 0$), the starting time of the NVT simulations (2, $t = 250$ ns), and the final configuration of the simulations (3, $t = 1.25$ μs). PLC molecules are shown in green (nPLC) and red (pPLC) and lipids in blue. Water sites were removed for clarity. Snapshots were built using the VMD program.[31]

the PLC protonation state and on where we added PLC molecules to the initial configuration. In two cases, PLC molecules, neutral or protonated, were randomly added to the external water phase. In the third case, the starting configuration had pPLC molecules randomly placed inside the membrane. Counterions were always added randomly in the water phase to compensate the pPLC charge. In order to differentiate between the two starting configurations containing pPLC, we will refer to them as pPLC-O (pPLC-I), i.e., pPLC placed outside (inside) the vesicle. nPLC-O refers to the starting configuration with the nPLCs outside.

In Figure 3a, we plot three snapshots taken during the nPLC-O run. Snapshot 1 corresponds to the initial configuration with nPLC molecules randomly distributed in the water phase. The other two snapshots were taken at the end of the NPT equilibration run ($t = 250$ ns) and at the end of the NVT run ($t = 1.25$ μs). Snapshots 2 and 3 clearly show that most of the nPLCs quickly diffused into the vesicle during the equilibration period, and remained inside during the whole simulation time, showing the big affinity of nPLC for the lipid phase. Results for the pPLC-O system indicate (snapshots not shown) that during the simulation time just a fraction of pPLC enters the vesicle. As for the case of pPLC-I, we found that many drug molecules leave the vesicle during the equilibration period, as shown by snapshots in Figure 3b taken at the same time as the ones in Figure 3a.

We calculated the number of PLC molecules absorbed by the vesicle as a function of time using as external vesicle radius the averaged over the NVT simulation time radius $\langle r_{ext} \rangle = 75.0$ Å. In Figure 4, we plot the number of PLC molecules inside the vesicle (i.e., within $\langle r_{ext} \rangle$) as a function of time for nPLC-O, pPLC-O, and pPLC-I. All systems reach equilibrium quite quickly. Nearly all (96%) of the 88 nPLC molecules are

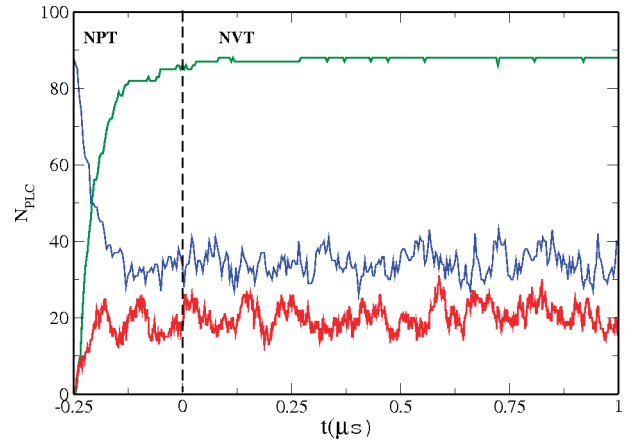

Figure 4. Number of PLC molecules inside the vesicle as a function of time: nPLC-O (green); pPLC-O (red); pPLC-I (blue).

absorbed within 100 ns. For the pPLC cases, the number of pPLC molecules within the vesicle is considerably smaller: an average of 20 ± 4 molecules for the pPLC-O case and 35 ± 7 for the pPLC-I case. The number of pPLC molecules inside the vesicle is considerably higher for the pPLC-I case than for the pPLC-O case, suggesting that at low pH liposome−PLC complexes could strongly depend on the preparation procedure, as quantified below.

We extended eq 1 for the case of a spherically symmetric object. We define the radial electron density profile as

$$\mathrm{REDP}(r) \propto \left\langle \frac{Q(r)}{4/3\pi((r+\delta)^3 - (r)^3)} \right\rangle_t \qquad (2)$$

where $Q(r)$ is the sum of the nuclear charge of all sites found between r and $r + \delta$. In Figure 5, we show the REDP of the

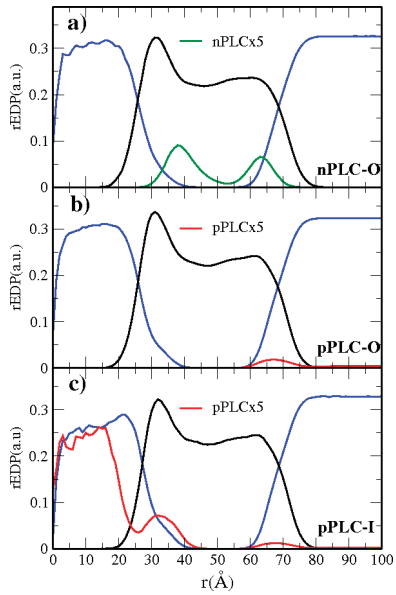

Figure 5. Radial electron density profile (REDP) of the different components of the nPLC/vesicle as a function of the r coordinate; $r = 0$ corresponds to the vesicle center. The colors are blue for water, black for POPC, green for neutral PLC, and red for pPLC. (a) nPLC; (b) pPLC-O (PLCs initially in water phase); (c) pPLC-I (PLCs initially in vesicle). The EDP of PLC was amplified 5 times for visualization purposes.

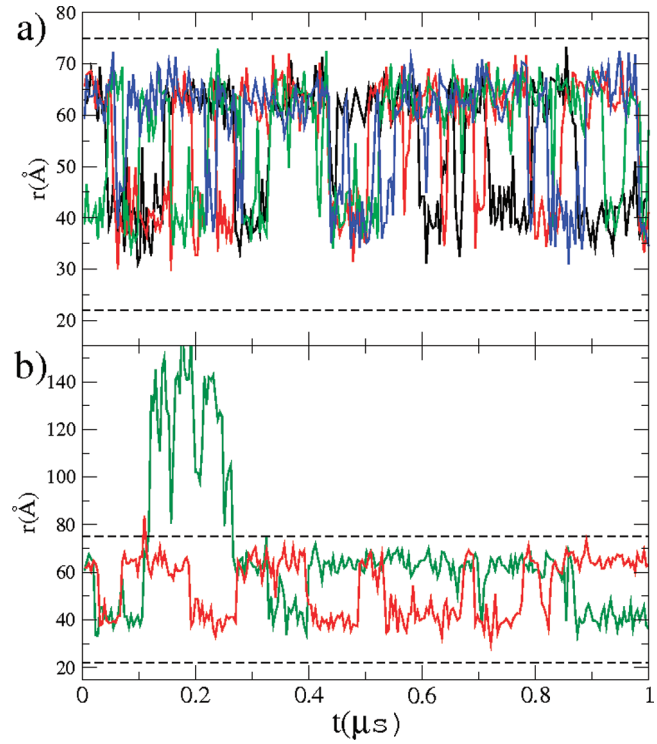

Figure 6. (a) Selected trajectories of the center of mass of four representative neutral PLCs. PLCs flip-flop between inner and outer vesicle layers with a frequency of $(15 \pm 2)/\mu$s. (b) Trajectories of the only two neutral PLCs leaving the vesicle during simulation, readily reabsorbed in less than 200 ns. The dashed lines indicate the inner and outer vesicle radii.

different systems under study: (a) nPLC-O, (b) pPLC-O, and (c) pPLC-I derived from the 1 μs NVT simulations. PLC densities have been magnified 5 times for visualization purposes (see caption for color details). Our simulation results show that for all three cases the lipid density has a higher density around the inner monolayer. This was also found by Risselada et al.[30] using fully equilibrated structures, which shows how our simulation setup also captures, at least qualitatively, the features pertaining to fully equilibrated vesicles. Lipid density asymmetry is a consequence of the bilayer curvature that allows more volume per tail to lipids docking on a concave shape, i.e., the inner monolayer. This argument applies also to the drug REDP, with nPLC molecules still following a bimodal distribution as observed for the case of flat bilayers (see section 3.1), with on average 34 (54) PLCs molecules in the internal (external) monolayer. This leads to an asymmetric bimodal drug distribution with higher nPLC:lipid ratio for the internal monolayer (0.13) with respect to the external one (0.08). The higher drug affinity of the inner shell arises from its lower lipid tail density (discussed above) and is reflected in a stress distribution across the bilayer.[10]

We stress here that, for bigger vesicles as the ones used experimentally, curvature effects are likely to be less pronounced. However, even with CG models, it is difficult to reach length scales of experimental structures.

Comparison between Figure 5b and c shows that for pPLC the distribution strongly depends on the initial conditions. We found that in the pPLC-O case the majority (77%) of pPLC distributes in the external water phase with the remaining 23% absorbed by the outer lipid shell. On the other hand, the pPLC-I distribution has two peaks inside the vesicle (at the lipid/water interface) and the rest of the pPLCs are distributed in the internal and external water regions. For pPLC-I, the average number of molecules in the external (internal) water phase was 27 (16), while 21 (14) molecules were attached to the external (internal) lipid monolayers. We point out that 42% of the pPLC molecules are in the external water phas; however, it is difficult to visualize it in the REDP because of the low radial density in the external water phase. The number of pPLCs found in the external monolayer starting from a pPLC-I configuration are in good agreement with the average pPLC number of the pPLC-O case. The rest of the pPLC molecules are distributed between the internal water phase and the inner lipid monolayer.

In order to elucidate the absorption process for the different starting cases, the dynamical behavior of PLC molecules was studied following the time evolution of the individual PLC center of mass distance $r(t)$ to the vesicle center. In Figure 6a, we show the trajectories of four selected nPLCs. nPLCs are found to cross between the monolayers (flip-flop, or crossing events) many times within the microsecond time scale. This behavior is representative of the great majority of the PLCs. The average rate of crossing events is high ($\sim 15 \pm 2$ times per molecule per microsecond), which suggests an unspecific interaction between vesicle lipids and neutral PLC that confines nPLC in the lipid membrane as a consequence of its hydrophobicity. As a matter of fact, only two molecules leave the vesicle diffusing into the water phase during the whole 1 μs run, one of them entering again into the vesicle almost immediately, and the other one within 0.2 μs. We show the center of mass trajectories of these two molecules in Figure 6b. On the other hand, for pPLC, we do not see any crossing events between the two monolayers during the whole length of our simulations. All pPLCs have instead a fast exchange with the water phase, as they leave and enter again into the vesicle many times (an average number of 4.5 ± 1.5 jumps/molecule) during the simulation time, as shown in Figure 7 for three selected pPLCs from the pPLC-O case. For the pPLC-I case, the molecules initially placed in the inner monolayer remain there or in the internal water region, with the average number of pPLCs in the external monolayer equal to 20. This explains

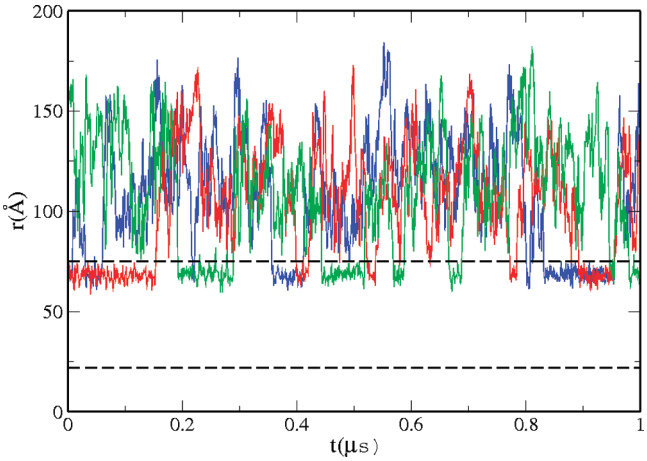

Figure 7. Selected trajectories of the center of mass of three representative pPLCs. The dashed lines indicate the inner and outer vesicle radii.

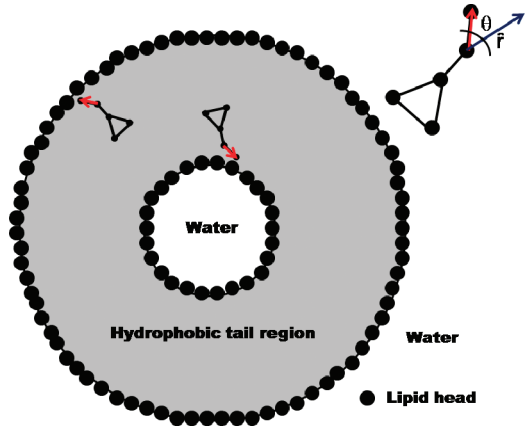

Figure 8. Schematic representation of the pPLC orientation inside the vesicle.

the different number of pPLCs inside the vesicle shown in Figure 4 and suggests that at low pH, when the PLC are protonated, liposome−PLC complexes can strongly depend on the preparation procedure. It is important to point out that the equilibrium between neutral and protonated species is dynamical. On the basis of our results, neutral molecules are able to cross membranes and protonated molecules have a fast exchange with water. In this way, the interplay between these two species seems fundamental for the encapsulation/delivery process as well as for the anesthesia mechanism.

In order to study the arrangement of absorbed PLC molecules in the vesicle, we measure θ, the angle formed by $\vec{T}_2-\vec{T}_1$ with the radial versor $\hat{r}$ in the system of reference with the origin in the vesicle center (see Figure 8 for details).

In Figure 9, we plot θ as a function of the molecule center of mass distance to the vesicle center, for all of the pPLC-I molecules over the whole NVT simulation run. From this figure, we can see that in water (22 Å $< r <$ 75 Å) all angles are sampled. However, for PLCs inside the vesicle, we found that the vector $\vec{T}_2-\vec{T}_1$ always points to the lipid heads, showing a specific orientation. Similar results, but only in the external monolayer, are found for the pPLC-O case (not shown). We therefore conclude that the pPLC molecules exhibit a preferential orientation when adsorbed to the vesicle inner and outer shells. This specific orientation is due to the pPLC amphiphilic character. The polar tails point to the lipid heads, while the hydrophobic ring enters deeper into the lipid hydrophobic core.

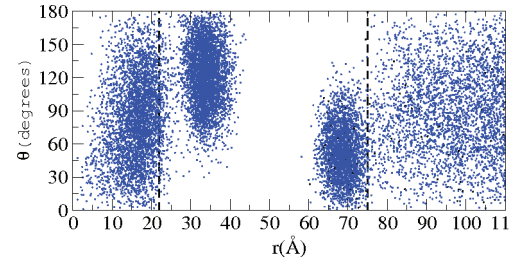

Figure 9. Mapping of θ (see text) vs $r(t)$ center of mass distance from the vesicle center for all of the protonated PLC over the 1 μs simulation run (pPLC-I case). The dashed lines indicate the inner and outer vesicle radii.

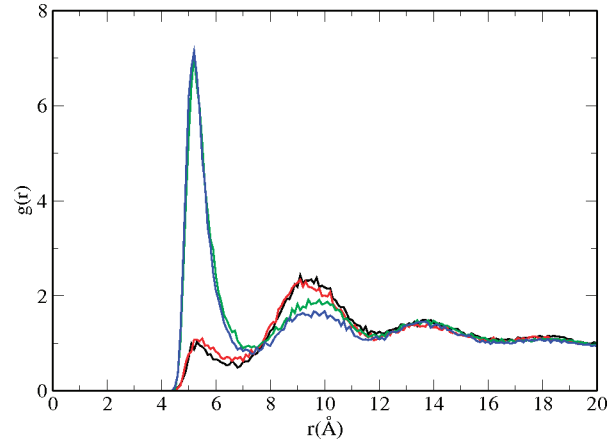

Figure 10. Radial distribution function, $g(r)$, between NC3 and T1 and T2 in black and red, respectively, and between PO4 and T1 and T2 in green and blue (NC3 and PO4 are the charged groups of the POPC head).

On the contrary, no preferential orientation was found for the neutral PLC in the POPC lipid tails, as found for the case of a flat lipid bilayer. This confirms the unspecific character (see above) of nPLC interaction with membrane.

The preferential orientation found for the pPLC molecule suggests a preferred insertion mechanism of the protonated drug on the vesicle layers which results from the interaction between the lipid heads and the charged groups of pPLC tails. We plot in Figure 10 the radial distribution function $g(r)$ of the charged lipid groups (PO4, NC3) and pPLC tail moieties ($T1$, $T2$) for the pPLC-O case. The peaks between the negatively charged site of the POPC head (PO4) and both positively charged sites of the pPLC tail found at ∼5 Å show a strong correlation, i.e., a preferred structural arrangement, as a result of the specific interaction between oppositely charged groups. Similar results are found for the pPLC-I case, while no correlation was found for the neutral case (not shown).

We therefore conclude that, although electrostatic interactions due to pPLC charged tail groups permit structured membrane−drug complexes to be built, the presence of charge on the pPLC tails effectively increases pPLC water affinity, leading to an overall decrease of the total absorption of pPLC, as electrostatic interaction between charged lipid heads and charged pPLC tails is not strong enough to trap the pPLCs permanently into the vesicle.

4. Conclusions

In this work, we studied the encapsulation of a local anesthetic, prilocaine, in a small liposome by means of coarse grained molecular dynamics. We employed a recently developed

coarse graining model, the MARTINI force field,[11] to model water and lipids. Prilocaine force field parameters were derived within the framework of MARTINI, and this extended force field was validated comparing coarse grained simulation results with fully atomistic simulation results of prilocaine embedded in a flat lipid bilayer. The use of a coarse grain model allowed us to reach relevant time and length scales of drug diffusion and membrane docking−undocking processes, otherwise impossible to observe using fully atomistic molecular dynamics.

Prilocaine can be found neutral or protonated under physiological conditions; therefore, we studied both cases. At equilibrium, chloride counterions are spread between the internal and external water phases, and the majority of protonated drug molecules do not attach or enter the vesicle, while a minority interacts with the membrane, performing fast attaching−detaching cycles involving different drug molecules. Neutral prilocaine is instead quickly (less than 200 ns) fully absorbed in the interior part of the lipid membrane where it adopts an asymmetric bimodal distribution. Further inspection reveals a structured interplay between protonated prilocaine and vesicle membrane, with protonated prilocaine tail groups arranging near the oppositely charged lipid heads. On the other hand, no preferential orientation or structure was found for absorbed neutral prilocaine. Our simulation results therefore suggest that, although protonation leads to a structured interaction between drug and host, hydrophobicity is the major driving force of drug encapsulation. Our results also show a dependence of the protonated PLC distribution on the preparation conditions, as the percentage of prilocaine molecules embedded into the liposome strongly varies depending on the initial conditions. This observation suggests that different preparation schemes of liposome−drug complexes leading to prilocaine trapped within vesicles could increase overall drug power.

Acknowledgment. We thank Ignacio Pagonabarraga and Marco D'Abramo for a critical reading of the paper and Eneida de Paula for helpful discussions. G.G. acknowledges support from the IEF Marie Curie scheme, and M.P. thanks FAPESP (06/02523-7) for financial support.

References and Notes

(1) Chorny, M.; Levy, R. J. *Proc. Natl. Acad. Sci. U.S.A.* **2009**, *106*, 6891–6892.
(2) Allen, T. M.; Cullis, P. R. *Science* **2004**, *303*, 1818–1822.
(3) Samad, A.; Sultana, Y.; Aqil, M. *Curr. Drug Delivery* **2007**, *4*, 297–305.
(4) Cereda, C. M. S.; Brunetto, G. B.; de Araujo, D. R.; de Paula, E. *Can. J. Anesth.* **2006**, *53*, 1092.
(5) Pickholz, M.; Oliveira, O. N.; Skaf, M. S. *Biophys. Chem.* **2007**, *125*, 425–434.
(6) Koubi, L.; Saiz, L.; Tarek, M.; Scharf, D.; Klein, M. L. *J. Phys. Chem. B* **2003**, *107*, 14500–14508.
(7) de Paula, E.; Schreier, S.; Jarrell, H. C.; Fraceto, L. F. *Biophys.Chem.* **2008**, *132*, 47–54.
(8) Stephenson, B.; Rangel-Yagui, C.; Pessoa, A.; Tavares, L.; Beers, K.; Blankschtein, D. *Langmuir* **2006**, *22*, 1514–1525.
(9) Toth, R.; Ferrone, M.; Miertus, S.; Chiellini, E.; Fermeglia, M.; Pricl, S. *Biomacromolecules* **2006**, *7*, 1714–1719.
(10) Marrink, S. J.; de Vries, A. H.; Tieleman, D. P. *Biochim. Biophys. Acta* **2009**, *1788*, 149–168.
(11) Marrink, S. J.; Risselada, H. J.; Yefimov, S.; Tieleman, D. P.; de Vries, A. H. *J. Phys. Chem. B* **2007**, *111*, 7812–7824.
(12) Marrink, S. J.; Mark, A. E. *J. Am. Chem. Soc.* **2003**, *125*, 15233–15242.
(13) Marrink, S. J.; Mark, A. E. *J. Am. Chem. Soc.* **2003**, *125*, 11144–11145.
(14) Wong-Ekkabut, J.; Baoukina, S.; Triampo, W.; Tang, I. M.; Tieleman, D. P.; Monticelli, L. *Nat. Nanotechnol.* **2008**, *3*, 363–368.
(15) Yefimov, S.; van der Giessen, E.; Onck, P. R.; Marrink, S. J. *Biophys. J.* **2008**, *94*, 2994–3002.
(16) Periole, X.; Huber, T.; Marrink, S. J.; Sakmar, T. P. *J. Am. Chem. Soc.* **2007**, *129*, 10126–10132.
(17) Orsi, M.; Sanderson, W. E.; Essex, J. W. *J. Phys. Chem. B* **2009**, *113*, 12019–12029.
(18) Michel, J.; Orsi, M.; Essex, J. W. *J. Phys. Chem. B* **2008**, *112*, 657–660.
(19) Hinner, M. J.; Marrink, S. J.; de Vries, A. H. *J. Phys. Chem. B* **2009**, *113*, 15807–15819.
(20) Butterworth, J. F.; Strichartz, G. R. *Anesthesiology* **1990**, *72*, 711–734.
(21) Marrink, S. J.; de Vries, A. H.; Mark, A. E. *J. Phys. Chem. B* **2004**, *108*, 750–760.
(22) Kasson, P. M.; Pande, V. S. *PLoS Comput. Biol.* **2007**, *3*, 228–2238.
(23) Monticelli, L.; Kandasamy, S. K.; Periole, X.; Larson, R. G.; Tieleman, D. P.; Marrink, S. J. *J. Chem. Theory Comput.* **2008**, *4*, 819–834.
(24) Pickholz, M.; Fraceto, L. F.; de Paula, E. *Int. J. Quantum Chem.* **2008**, *108*, 2386–2391.
(25) Cabeça, L. F.; Pickholz, M.; de Paula, E.; Marsaioli, A. J. *J. Phys. Chem. B* **2009**, *113*, 2365–2370.
(26) http://md.chem.rug.nl/~marrink/MARTINI/Coordinates.html.
(27) Risselada, H.; Mark, A.; Marrink, S. *J. Phys. Chem. B* **2008**, *112*, 7438–7447.
(28) Hess, B.; Kutzner, C.; van der Spoel, D.; Lindahl, E. *J. Chem. Theory Comput.* **2008**, *4*, 435–447.
(29) Smith, G. S.; Majewski, J. X-ray and neutron studies of lipid bilayers. In *Lipid Bilayers, Structure and Interactions*; Katasaras, J., Gutberlet, T., Eds.; Springer: Berlin, Germany, 2000.
(30) Risselada, H. J.; Marrink, S. J. *Phys. Chem. Chem. Phys.* **2009**, *11*, 2056–2067.
(31) Humphrey, W.; Dalke, A.; Schulten, K. *J. Mol. Graphics* **1996**, *14*, 33–38.

JP909148N